Available online at sjuoz.uoz.edu.krd

Science Journal of University of Zakho

Vol. 11, No. 4, pp. 548 – 556 October-Dcember, 2023

p-ISSN: 2663-628X
e-ISSN: 2663-6298

journals.uoz.edu.krd

CHARACTERIZATION OF SYNTHESIZED SILVER NANOPARTICLES USING LEPIDIUM SATIVUM PLANT

Jilan Obaidellah[1], Sabah M. Ahmed[2]

1,2 College of Science, University of Duhok, Kurdistan Region, Iraq - (jilan.noor, sabma62)@uod.ac

Received: 14 Jul., 2023 / Accepted: 12 Sep., 2023 / Published: 10 Dec., 2023. https://doi.org/10.25271/sjuoz.2023.11.4.1174

ABSTRACT:
The biosynthesis of Silver Nanoparticles (Ag NPs) was achieved through the utilization of an extract derived from the plant Lepidium Sativum, commonly referred to as Garden cress. The current study was undertaken to examine the impacts of different concentrations of silver nitrate (AgNO3) (0.1, 0.15, 0.2, 0.25, and 0.3) on the properties of silver nanoparticles. A range of analytical techniques were utilized to examine the characteristics of the nanoparticles, encompassing energy dispersive X-ray (EDX), field emission scanning electron microscopy (FESEM), UV-visible spectrophotometry (UV-Vis), X-ray diffraction (XRD), and Fourier-transform infrared spectroscopy (FTIR). The findings demonstrated and suggested that Lepidium Sativum represents a viable choice for the environmentally friendly production of silver nanoparticles. The UV-Vis spectra of the studied silver nanoparticles (Ag NPs) exhibited a significant level of absorption within the wavelength range of 430-460 nm. The most intense absorption peak, observed at 453 nm, was associated with a concentration of 0.25 mol. The examination of the Field Emission Scanning Electron Microscope (FESEM) images has revealed that the concentration of the solution has a substantial impact on the size, morphology, shape, and orientation of the silver nanoparticles (Ag NPs). The Ag NPs exhibit a mostly spherical and semi-spherical form, with an average particle size ranging from 65 to 80 nm. Additionally, the X-ray diffraction (XRD) analysis revealed that the silver nanoparticles (Ag NPs) synthesized exhibit a high level of purity, consisting solely of silver atoms arranged in a face-centered cubic crystalline lattice structure. The particle size, as determined from the (111) peak, falls within the range of 25.31-67.28 nm. The EDX spectrum analysis indicated that the primary chemical constituent present in the samples was silver (Ag). The silver nanoparticles (Ag NPs) produced at different concentrations exhibited a distinct peak in the UV-Vis spectrum, demonstrating significant absorbance above 400 nm in the visible region and minimal absorption in the UV range. The measured energy band gap (Eg) ranged from 2.05 to 2.3 eV. In addition, the Fourier Transform Infrared (FTIR) spectra of silver nanoparticles (Ag NPs) at different concentrations did not exhibit any discernible peak throughout the monitored range. This observation implies that the silver nanoparticles that were produced using cress plant extract had a high level of purity.

KEYWORDS: Silver nanoparticles, Nanoparticles, Lepidium Sativum, Plant extraction, green synthesis

1. INTRODUCTION:

Nanotechnology is an emerging field of study that is now in its nascent phase. This can affect a lot of things. Nanomaterials are tiny pieces of materials that are very small, which means that they can be used for a lot of different purposes. They have gained a large interest from scientist in both, applied science as well as in basic. Recently scientists have given a great interest to silver nanoparticles. Ag NPs have some unusual properties that make them useful in a variety of fields, including biomedical research (imaging, fast diagnosis, tissue regeneration, and drug delivery[0], textile industry[0], food packaging[0], cosmetic industry[0], catalysis[0], sensors[0], coatings[0], Plasmonics (SERS)[0], optoelectronics[0], antimicrobial activities[0], DNA sequencing[0], contamination control and climate change[0], clean water technology[0], information storage, and energy generation. Ag NPs are very conductive, which has made them useful in electronic devices, inks, adhesives, and other materials[0]. Several bottom-up-approach techniques such as bio-reduction (plants, fungi, bacteria, yeast, biopolymers), sono-chemical, chemical reduction, photochemical, microemulsion, electrochemical, microwave, pyrolysis, Coprecipitaion and as well as top-down-approach techniques such as Evaporation-condensation, pulsed laser ablation, Ball-milling, Spray-pyrolysis, vapor-and-gas phase have been implemented for the synthesis of silver NPs[0]. It has been revealed that biological methods are cheaper and more active, cleaner and safer than other methods[0].

The nanoparticles generated by biosynthesis method have more defined sizes and shapes than other physiochemical methods[0]. Biological systems use natural chemicals to help keep nanoparticles stable. These chemicals act as capping agents, pushing the nanoparticles in the desired direction. A literature review indicates that plants offer many advantages over other biological systems. Since plant extracts make it easy to form nanoparticles, these particles are more stable than those made from chemicals[0].

Plant components such as leaf, stem, seed, and root are frequently utilized in the creation of metal-based nanoparticles. There are several components in the plant extract, including phenolic acids, terpenoids, proteins, carbohydrates, bioactive polyphenols, and alkaloids. These substances work together reduce metallic ions and help to keep them stable[0]. Plant NPs biosynthesis occurs in three phases: reduction, growth, and stabilization[0]. Reducing agents are important in recovering metal ions from salt precursors. During the reduction phase, biomolecules help to reduce the metal ions. The metal ions change from a single type of atom to two different types of atoms as they move around. This happens because oxidation happens, which makes the metal ions become more different in size. Then, small bits of metal (called "reduced metal atoms") start to form. During growth, when metal atoms recombine to form metal

* Corresponding author

Available online at sjuoz.uoz.edu.krd

journals.uoz.edu.krd

Science Journal of University of Zakho

Vol. 11, No. 4, pp. 548 – 556 October-Dcember, 2023

p-ISSN: 2663-628X
e-ISSN: 2663-6298

nanoparticles, but then quickly break down again into smaller pieces, metal ions undergo further biological reduction. Nucleation can help to form larger clusters of nanoparticles, but the growth phase makes the nanoparticles more stable and allows them to form more different shapes.

The last step is the stabilization phase in which the nanoparticles are made smaller and more stable by coating them with metabolites[0]. The quality, size, and shape of the biosynthesized NPs are impacted by a number of extra reaction conditions, like the reaction temperature and time, solutions pH, concentration of plant extract, concentration of metal salt[0]. One of the first approaches that were made with plants extract for the production of Ag NPs used *Alfalfa* sprouts[0]. It appeared to be a faster process in contrast to the utilization of fungus and bacteria, and the production of Ag NPs was more rapidly. Also, the plant *Geranium* leaf was used in research by Shankar et al. and it took only 9 hours to reach 90% reaction, this is very short time compared to further researches which took 24 to 124 hours[0].

Recently, scientists were able to create Ag NPs with very good antibacterial properties using *Chrysanthemum indicum L.*[0] and *acacia leucophloea*[0] extracts which have diameters that range from 38 to 72 nm, and 17 to 29 nm, respectively. Additionally, the plant *Ganoderma neojaponicum* is a species of fungus that belongs to the Ganoderma genus. The Imazeki method was employed for the manufacture of silver nanoparticles (Ag NPs), which were subsequently evaluated as possible cytotoxic agents against breast cancer cells. [0]. In this present study, the Ag NPs have been synthesized by using the plant extract of *Lepidium Sativum.* The effect of varying concentrations on the silver nanoparticles, which were manufactured using the green approach, was obtained and reported. The significance between the different concentrations on the Ag NP's quality and concentration that is more appropriate has been investigated. Ag NPs can be used for many uses such as; disinfectants, broad-spectrum microbicides, and wound care products.

2. Materials and Method:

The used chemicals are silver nitrate $AgNO_3$ from the company Biochem Chemopharma, which has a molecular weight of 169.88g/mol. It has a purity of 99.9% and sodium borohydride (NaOH) powder. For the synthesis of Ag NPs, a heater-stirrer (Model HS-12) and a pH meter (ECO Testr pH2) were utilized.

2.1. Preparation of the Lepidium Sativum plant:

Garden cress, derived from the old Germanic cresso, which means sharp, spicy, is commonly accessible around the world. It is an edible plant that grows quickly. Raw cress contains 89% water, 6% carbs (1% dietary fiber), 3% protein, and 1% fat. The plant was cleaned and allowed to dry after that. The plant water that was draining was then squeezed in a blender. Finally, 50g of the squeezed plant was combined with 50 ml of distilled water. This combination was heated at a temperature of 80^{O}C using the heater-stirrer until the plant seemed to have no extracted left to give to the water. The liquid was then filtered several times to make sure no impurities were left, and finally stored for future use.

2.2. Biosynthesis of Silver Nanoparticles (Ag NPs):

The Ag NPs have been prepared using the biosynthesis process and extract from *Lepidium Sativum* with silver nitrate ($AgNO_3$). After the plant extract was prepared, ($AgNO_3$) was added to another 50 ml of distilled water and stirred on the heater-stirrer for about 20 minutes. Drop by drop, the produced extract was added to the solution of silver nitrate ($AgNO_3$). Furthermore, the pH of this mixture was controlled to 8 by adding Sodium Hydroxide (NaOH) to the mixture. This mixture was kept stirred at 80^{O}C until it had a consistency like thick liquid (paste). After that, the paste was put into a porcelain crucible with a volume of 50 ml and kept on the heater at a high temperature. Finally, Ag NPs were prepared (Figure 1). This procedure was done several times for different concentrations of silver nitrate (0.1mol, 0.15mol, 0.2mol, 0.25mol, 0.3mol). The given concentrations above were applied to Equation (**1**, which gave the exact amount of silver nitrate in grams that had to be added to the distilled water. The NPs powder was then washed with ethanol in order to remove any contaminants. Finally, the samples were put in a furnace for about 2 hours at a temperature of 500^{O}C (calcination temperature), where the silver nanoparticles were obtained.

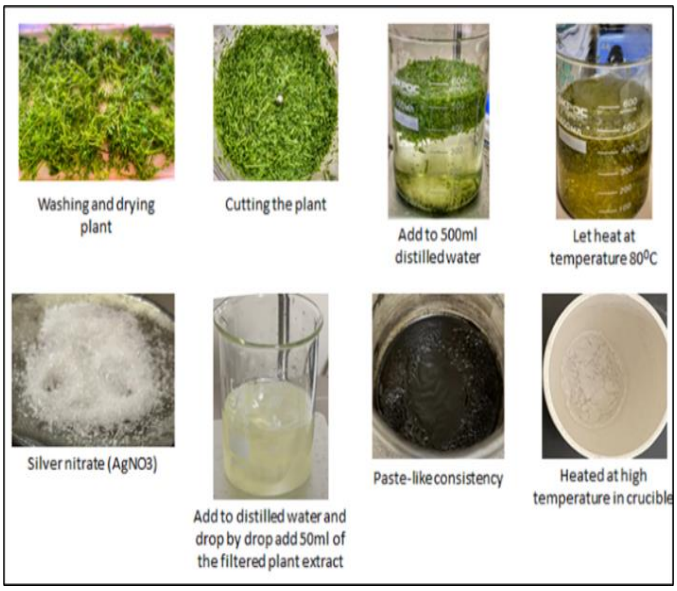

Figure 1: Schematic representation of Ag NPs for biosynthesis of Lepidium Sativum leaf exract in addition to the $AgNO_3$ salt

$$\boldsymbol{weight(gm) = MW(AgNO3)(\frac{gm}{mol}) \times M(mol) \times \frac{V}{1000ml}} \quad (1)$$

Where MW = molecular weight
M = molarity
V = the volume of the distilled water (ml)

2.3. Characterization of Ag NPs:

The optical characteristics of Ag NPs have been characterized using the Agilent Technologies Carrier Series UV-Visible double-beam spectrophotometer (FTIR), specifically the Cary 100 UV-Vis model. The Fourier Transform Infrared Spectroscopy technique has been applied to analyze the Lepidium Sativum extract and Ag NPs synthesized with different concentrations of Silver Nitrate (AgNO3). The FTIR analysis was conducted using a Nicolet IS 10 instrument manufactured by

* Corresponding author

Available online at sjuoz.uoz.edu.krd

journals.uoz.edu.krd

Science Journal of University of Zakho

Vol. 11, No. 4, pp. 548 – 556 October-Dcember, 2023

p-ISSN: 2663-628X
e-ISSN: 2663-6298

Thermo Scientific, located in Waltham, MA, USA. The spectral range examined was 400-4000 cm-1.

Ag nanoparticles were characterized and analyzed for their surface properties, size, shape, chemical composition, and orientation using energy-dispersive X-ray spectroscopy (EDX) and field emission scanning electron microscopy (FE-SEM) with an acceleration voltage ranging from 5 to 30 kV. The instrument utilized for this analysis was the Carl Zeiss AG Supra 55VP. The investigation focused on examining the strain, size, stress, crystal structure, epitaxial growth quality of Ag nanoparticles (NPs) created using the Pro MRD, PAN X-Pert high-resolution X-ray diffraction (HR-XRD) system model. The quantities of silver nitrate (AgNO3) were varied in order to assess their impact on these properties. The wavelength of CuK radiation is measured to be 1.54050 angstrom, while the scanning angle ranges from 20 to 80 degrees.

Table 1 Lattice parameters of Ag wurtzite FCC structure characteristics at strong diffraction peaks for the (111), (200), (220), and (311) planes of Ag NPs produced with various $AgNO_3$ concentrations.

Concentration	2θ	X-ray Peaks	d-spacing (Å)	FWHM	a (Å)	ε_a%
0.1	37.6	111	2.38	0.118	4.134	1.10
0.15	37.8	111	2.37	0.177	4.115	0.64
0.2	37.8	111	2.37	0.314	4.116	0.64
0.25	37.3	111	2.40	0.236	4.169	1.94
0.3	37.6	111	2.39	0.236	4.140	1.23
0.1	43.8	200	2.06	0.275	4.127	0.92
0.15	44.0	200	2.05	0.236	4.113	0.57
0.2	43.8	200	2.06	0.354	4.125	0.88
0.25	43.5	200	2.07	0.196	4.158	1.67
0.3	43.7	200	2.07	0.354	4.141	1.26
0.1	64.0	220	1.45	0.314	4.109	0.49
0.15	64.1	220	1.45	0.393	4.103	0.33
0.2	64.1	220	1.45	0.393	4.106	0.40
0.25	63.7	220	1.45	0.393	4.127	0.91
0.3	63.9	220	1.45	0.393	4.117	0.69
0.1	77.0	311	1.23	0.118	4.107	0.43
0.15	77.1	311	1.23	0.472	4.101	0.28
0.2	77.0	311	1.23	0.472	4.103	0.33
0.25	76.7	311	1.24	0.157	4.118	0.69
0.3	76.8	311	1.23	0.472	4.112	0.54

The above table contains results for the lattice constant (a), the strain (εa), and the inter-planar distance (d) along diffraction peaks (111), (200), (220), and (311) for Ag NPs synthesized by different concentration of silver nitrate. The two parameters a, and ε_a have been calculated by the equations **(2** and **Error! Reference source not found.**, respectively.

$$a = d \times \sqrt{h^2 + k^2 + l^2} \quad (2)$$

Where h, k, and l are x-ray diffraction peak miller indices.

$$\varepsilon_a = \frac{a - a_0}{a_0} \times 100\% \quad (3)$$

Table 2 The particle size (D), Volume (V), and bond length (L) of the dominant peaks at (111), (200), (220), and (311) planes of Ag NPs synthesized by different concentration of $AgNO_3$.

Concentration	X-Ray Peaks	D (nm)	V (Å^3)	L (Å)
0.1	111	67.28	70.69	2.92
0.15	111	45.01	69.72	2.91
0.2	111	25.31	69.73	2.91
0.25	111	34.13	72.46	2.94
0.3	111	33.66	70.97	2.92
0.1	200	28.88	70.31	2.91
0.15	200	33.65	69.59	2.90
0.2	200	22.45	70.22	2.91
0.25	200	41.43	71.90	2.94
0.3	200	22.63	71.01	2.92
0.1	220	31.16	69.42	2.90
0.15	220	26.01	69.09	2.90
0.2	220	25.52	69.23	2.90
0.25	220	22.73	70.29	2.91

* Corresponding author

Available online at sjuoz.uoz.edu.krd

Science Journal of University of Zakho

Vol. 11, No. 4, pp. 548 – 556 October-Dcember, 2023

p-ISSN: 2663-628X
e-ISSN: 2663-6298

journals.uoz.edu.krd

Table **2**.

$$D = \frac{k\lambda}{\beta cos\,\theta} \quad (4)$$

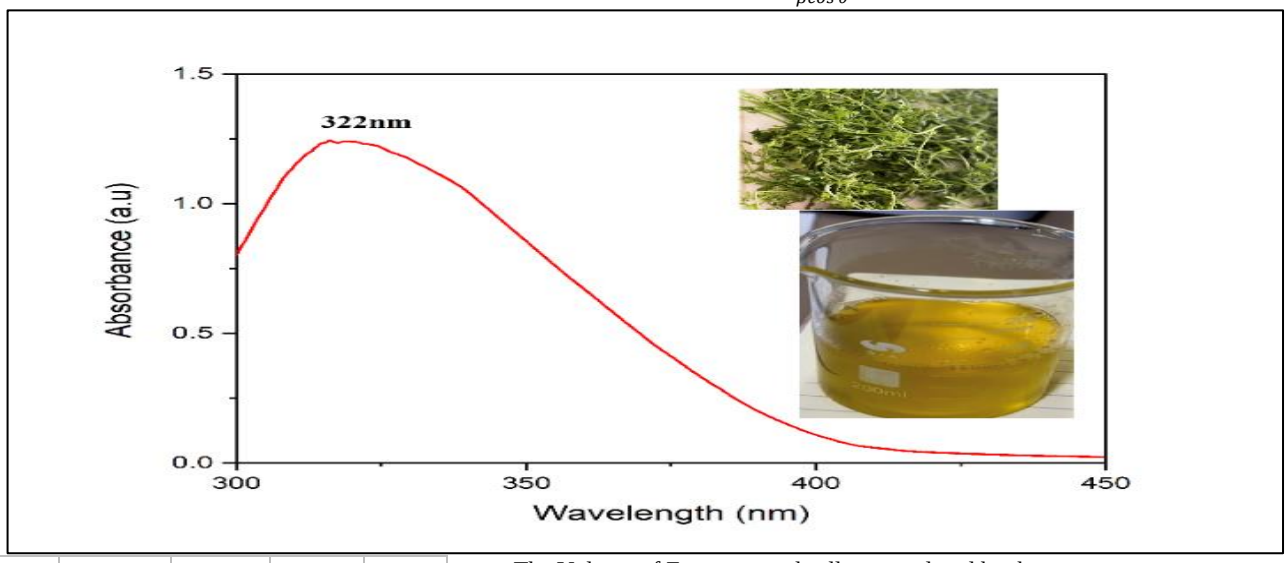

0.3	220	23.78	69.82	2.91
0.1	311	96.70	69.28	2.90
0.15	311	26.06	68.98	2.89
0.2	311	25.35	69.08	2.90
0.25	311	65.08	69.83	2.91
0.3	311	22.97	69.52	2.90

The average particle size of Ag NPs in the principal diffraction peaks was calculated using the Debye-Scherrer Equation (4, and the results are shown in

Figure 2). The spectrum's prominent and highest absorption peak, which is in the UV-region, is located at 322 nm.

The Volume of Face-centered cell was explored by the following equation (**5**.

$$\boldsymbol{V = a^3} \quad (5)$$

The Bond length (L) is defined as the distance between the centers of the two Atoms and is calculated by Equation (**6**. The Bond length results listed in

Table **2** represent how the change in concentration has effect on the bond length of Ag NPs along the diffraction peaks (111), (200), (220), and (311).

$$\boldsymbol{L = \frac{a}{\sqrt{2}}} \quad (6)$$

3. RESULTS AND DISCUSSION:

3.1. Characterization of Lepidium Sativum Plant Extract:

Metal ions in the plant extract are changed into metal nanoparticles by the phytochemicals. Additionally, the plant extract has reducing and stabilizing agents. This reaction's development was seen using UV-Vis' spectra (

Figure 2: The UV-Visible spectrum of Lepidium Sativum plant extract.

* Corresponding author

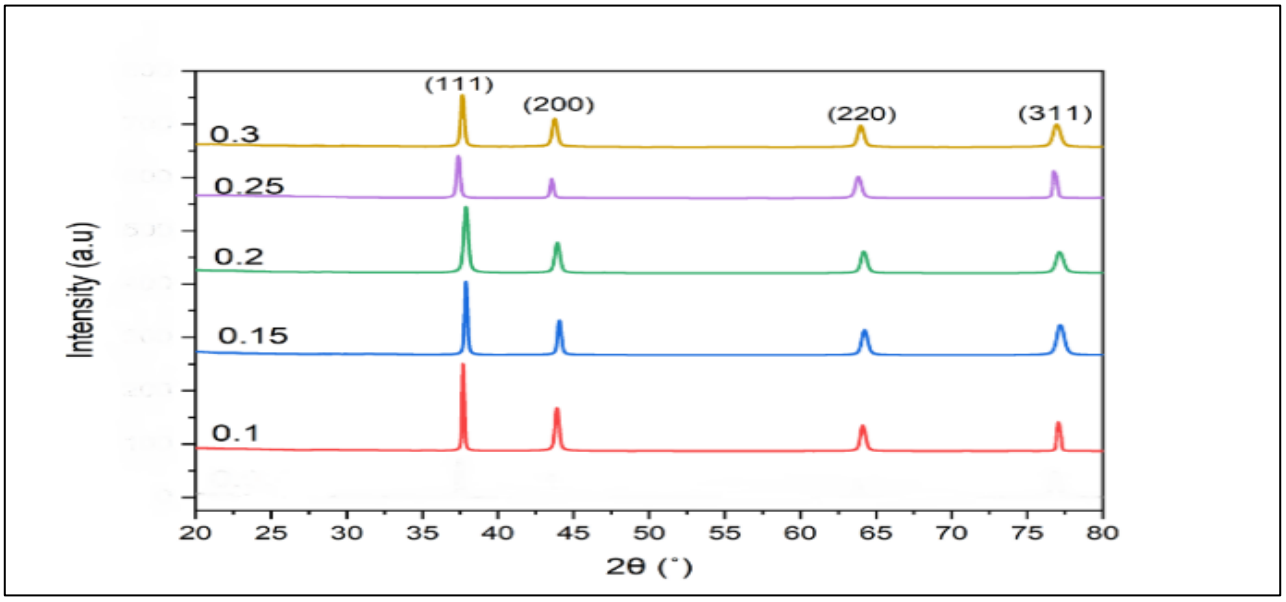

Figure 3: The patterns obtained by XRD of Ag NPs generated utilizing the green approach and the plant extract of Lepidium Sativum at various concentrations.

3.2 Characterization of synthesized Ag NPs

3.2.1 The Analysis of X-Ray Diffraction

The X-Ray diffraction patterns of Ag NPs formed through the green synthesis method using *Lepidium Sativum* extract at different concentrations are demonstrated in Figure 3. The XRD diffraction pattern approves that the structure is crystalline face-centered cubic for Ag NPs and it is according to (JCPDS card No. 98-005-3762).

Due to the absence of any diffraction peaks that reveal impurities or defects, there is a proof for the purity of Ag Nano crystals relative to the resolution of the XRD system. Figure 3 demonstrates that the XRD patterns for all concentration display four prominent diffraction peaks (111), (200), (220) and (311). The highest intensity and dominant peak at (111) demonstrate the good crystalline character of produced Ag NPs by their sharp-narrow full width at half maximum (FWHM). The FWHM has been significantly affected by the rise in concentration. As a consequence, increasing the concentration strengthens the quality of the crystal structure while also influencing the size of the produced Ag NPs. However, the behavior of the XRD patterns at varied concentrations is consistent with previous research[0,0]. Along the dominant diffraction peak (111), the measured average particle sizes of the Ag NPs synthesized with concentrations of 0.1 mol, 0.15 mol, 0.2 mol, 0.25 mol, and 0.3 mol are 67.287 nm, 45.017 nm, 25.315 nm, 34.135 nm, and 33.662 nm, respectively measured using Equation (4. From the results it can be seen that for the diffraction peak (111), the best applied concentration of $AgNO_3$ was 0.2 mol, which gives a particle size of 25.315 nm, which is in good accord with prior studies[556,0,0].

Smaller particles have a greater surface area. For this reason, smaller particles have a better antibacterial effect[0], which is one of the leading properties of Ag NPs. Table 1 represents the structural features, such as intensity, peak position (θ), lattice constant (a), and internal strain (ε_a) of Ag NPs along the diffraction peaks (111), (200), (220), and (311). The change in concentration has a considerable effect on the calculated lattice constants and strain along diffraction peaks. From Table 1, one can predict that there are both types of deformations, compressive stresses and tensile stresses. The strain values represent lattice contraction and lattice expansion. It is clearly predictable from Table 1, that the inter-planar distance is strongly affected by changing the concentration.

3.2.2 The Analysis of Energy-dispersive X-ray Spectroscopy (EDX)

Figure 4 presents the chemical element results for biosynthesized Ag NPs made from cress plant extract with different molar concentrations. In addition, Figure 4 shows that an EDX analysis of the spectra of the synthesized Ag NPs showed that the main chemical component was silver. The EDX spectra revealed a prominent Ag peak at 3 keV, as one would anticipate from Ag NPs[0].

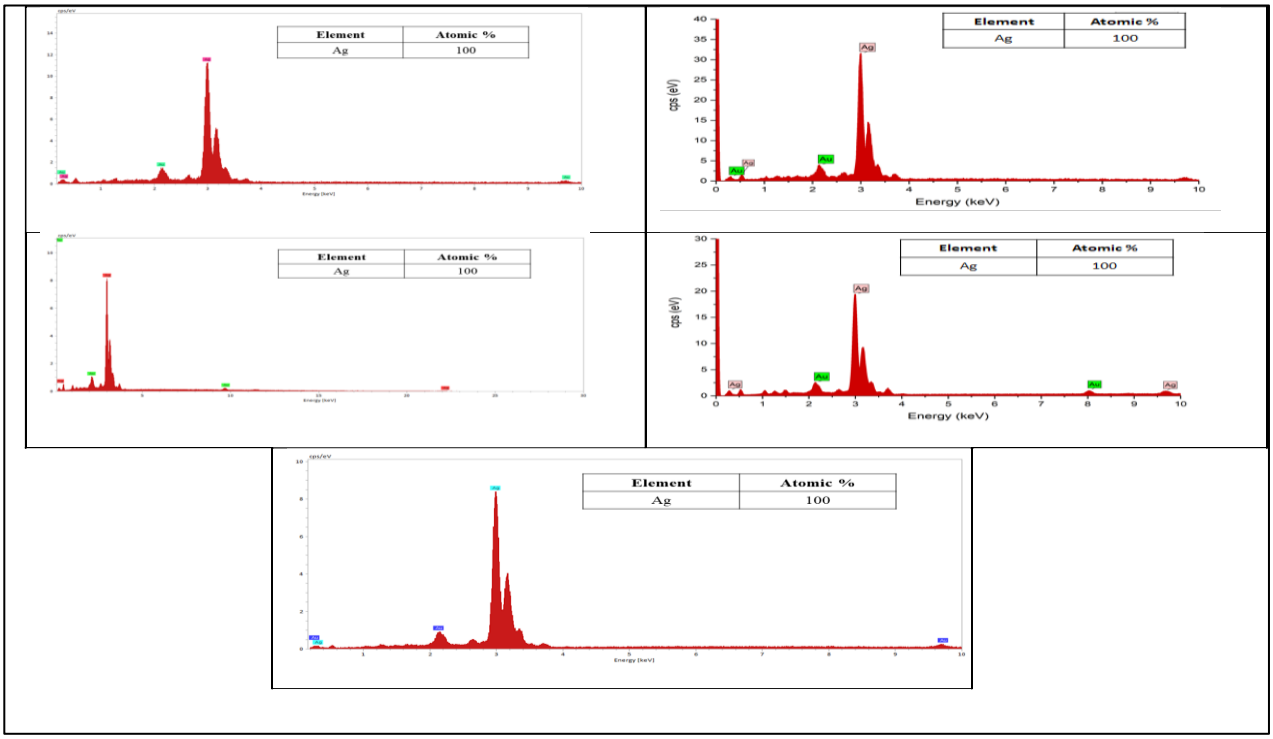

Figure 4: The EDX analysis of Ag NPs synthesized utilizing the green approach and plant extract of Lepidium Sativum at various silver nitrate concentrations.

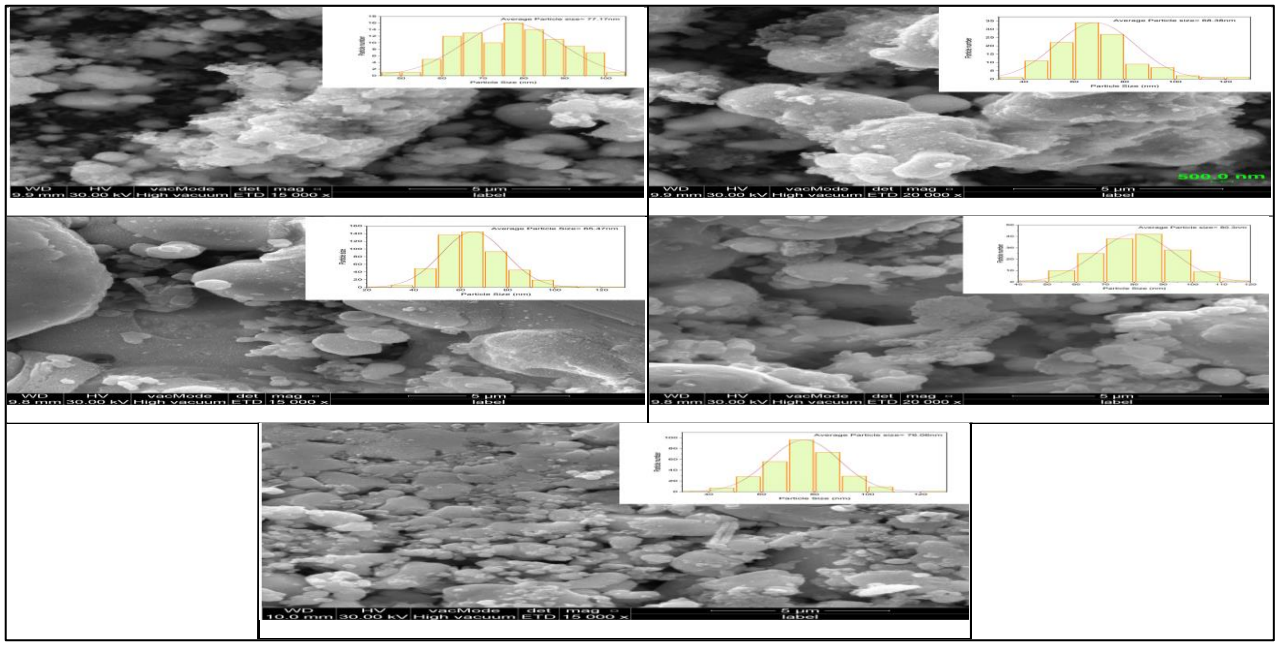

Figure 5: SEM top-view images of Ag NPs synthesized by using the green technique and cress plant extract in various concentration quantities at a calcination temperature of 500^{O}C.

3.2.3 *Field Emission Scanning Electron (FESEM) Microscopy:*

The size, surface morphology, orientation, shape, and distribution of biosynthesized Ag nanoparticles from silver nitrate salt have all been examined using the FESEM technique (**Error! Reference source not found.**), at different molar concentration of $AgNO_3$ salt.

The molar concentration of 0.1 mol is illustrated in Figure 5a, which shows Ag nanoparticles with a high-density distribution with a semispherical shape and an average particle size of 77.17 nm measured using ImageJ software.

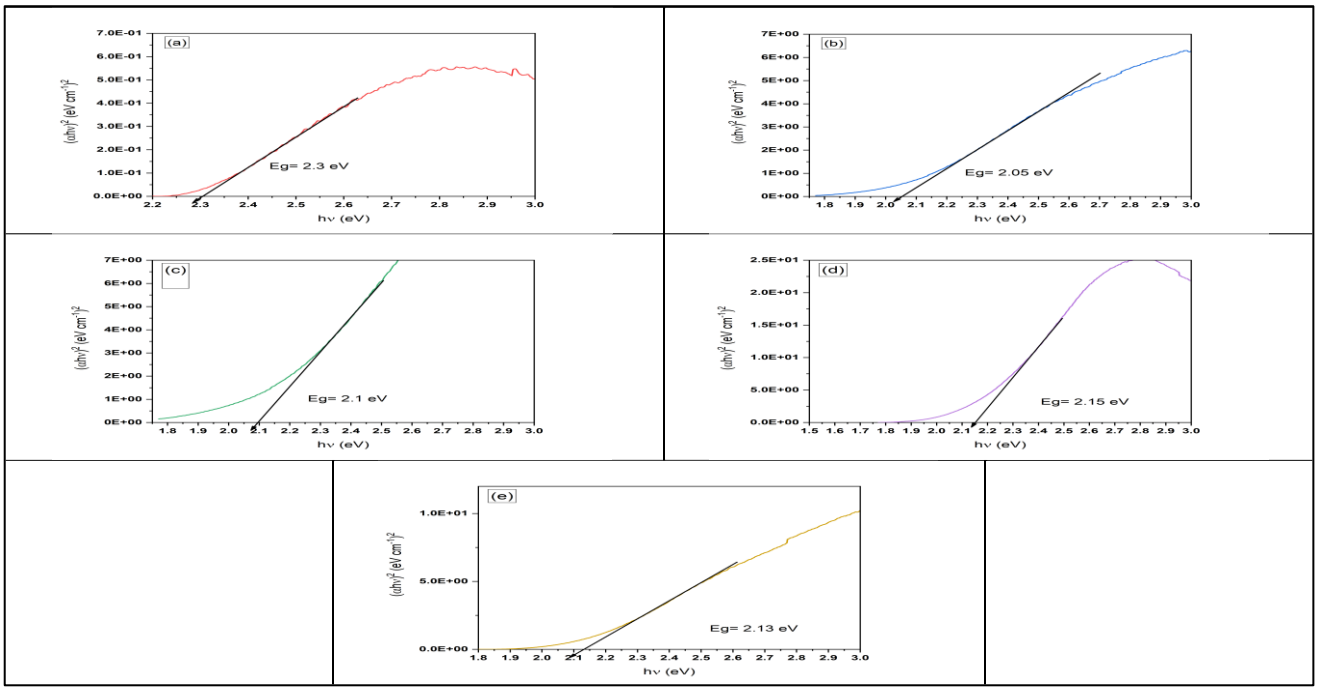

It is followed by Figure 5b, where the concentration was increased to 0.15 mol and some agglomeration is noticed with a mean particle size of 68.38 nm. Their shape also represents semi-spheres. The Ag nanoparticles shown in Figure 5c have been obtained with a molar concentration at 0.2 mol. the nanoparticles are spherical shaped, and the average particle size is around 65.47 nm. Furthermore, spherical shaped of Ag nanoparticles and low rate of aggregation are shown in Figure 5d with a molar concentration of 0.25mol. and the average particle size 80.3 nm.

Figure 6**:** Tauc plot [$(\alpha h\nu)^2$ vs. energy band gap (hv)] of Ag NPs produced utilizing green technique and the extract of the lepidium sativum plant with various concentrations.

Also, Figure 5e manifests the Ag nanoparticles obtained at a molar concentration of 0.3 mol with a particle size of 76.06 nm and a mostly uniform shape. Finally, as shown in **Error! Reference source not found.**, the bulk of the produced Ag nanoparticles had spherical or semispherical shapes. Occasionally, aggregation is formed which is a feature of green synthesis nanoparticles. This agglomeration comes from the large surface area and long-lasting affinities that biosynthesized nanoparticles have[0]. It might be suggested, that environmental conditions have a substantial impact on the stability and aggregation of NPs. As a result of the nanoparticles developing and the NPs joining together, asymmetrical clusters naturally emerge.

3.2.4 UV-Visible Spectroscopy Analysis[0].

The impact of of $AgNO_3$ concentration on the optical properties of the Ag NPs obtained from *Lepidium Sativum* plant extract were studied by the UV-Vis spectroscopy, as shown in The optical energy gap of the Ag NPs is illustrated in Figure 6 and it is around 2.15 eV. This value aligns with the anticipated optical energy gap for Ag NPs[0]. The band-gap energies of Ag NPs, as indicated by the concentrations depicted on the graph, are estimated to be 2.3 eV, 2.05 eV, 2.1 eV, 2.15 eV, and 2.13 eV, correspondingly.

Figure 7: The spectra obtained by UV-visible spectrophotometer for Ag nanoparticles synthesized utilizing the plant extract of Lepidium Sativum.

. It can be observed that there is a high absorption peak around 430-460 nm for all concentration values of $AgNO_3$. This absorption peak is considered to be in the visible range of UV-Vis spectra and the obtained results are agree with earlier

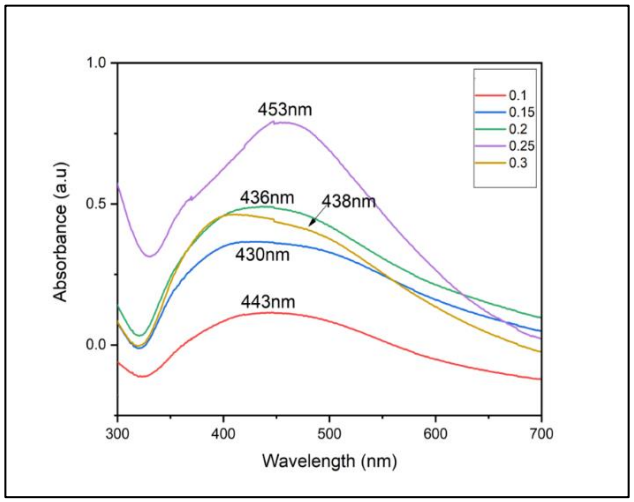

research[0,0]. The best result was given by the concentration value 0.25 mol of $AgNO_3$ with the highest absorption of approximately 80% at 453 nm wavelength. There were more molecules in the solution that interact and prevented light transmission as the concentration of AgNO3 increased.

The optical energy gap of the Ag NPs is illustrated in Figure 6 and it is around 2.15 eV. This value aligns with the anticipated optical energy gap for Ag NPs[0]. The band-gap energies of Ag NPs, as indicated by the concentrations depicted on the graph, are estimated to be 2.3 eV, 2.05 eV, 2.1 eV, 2.15 eV, and 2.13 eV, correspondingly.

Figure 7: The spectra obtained by UV-visible spectrophotometer for Ag nanoparticles synthesized utilizing the plant extract of Lepidium Sativum.

3.2.5. The Analysis of Fourier Transform Infrared Spectroscopy (FTIR)

The purity and composition of Ag NPs synthesized utilizing the green technique and plant extract of garden cress (Lepidium Sativum) with various concentrations were examined by the non-destructive method of FTIR spectra (

Figure 8).

All FTIR spectra, a sharp and strong peak at 1390 cm^{-1} is observed which represents O-H bending alcohol. Additionally, in all the above spectra manifest a sharp and medium peak in the region 790-840 cm^{-1}, which are C=C bending alkenes. A sharp peak appears in

Figure 8(d, e) at 1789 cm^{-1}, which is C=O stretching acid halide. C-N stretching amine is observed in

Figure 8(a) with the peaks 1109 cm^{-1} and 1176 cm^{-1}, and in

Figure 8(c) with the peaks 1184 cm^{-1} and 1132 cm^{-1}. These results agree with earlier research on Ag NPs[0,0]. However, some peaks may have vanished and some additional peaks may have been obtained, and the reason for this could be because of the quantum confinement.

Figure 8a depicts the FTIR spectrum of Ag NPs produced at a concentration value of 0.1 mol. At 1390 cm^{-1}, there is a sharp and strong absorption peak, representing the (O-H) bending alcohol. Two peaks (1109 cm^{-1} and 1176 cm^{-1}) in the range 1020-1250 cm^{-1} are present which represent the (C-N) stretching amine. Furthermore, the (C=C) bending alkene is responsible for the sharp peaks 873 cm^{-1} and 825 cm^{-1}. Moreover, the observed absorption peak at a wavenumber of 617 cm-1 can be attributed to the stretching of disulfide bonds (S-S).

Figure 8b depicts the Fourier Transform Infrared (FTIR) spectrum of Ag NPs synthesized with a concentration of 0.15 mol. Once again, a distinct peak of high intensity is observed at a wavenumber of 1390 cm^{-1}, it can be attributed to the bending motion of the (O-H) bond in the alcohol molecule. The presence of a distinct absorption peak at 837 cm^{-1} can be due to (C=C) bending motion in an alkene compound. The spectral peaks observed at 439 cm^{-1}, and 453 cm^{-1} correspond to stretching vibrations of aryl disulfide (S-S) bonds. Additionally, the peaks observed at 464 cm^{-1} and 482 cm^{-1} can be attributed to the stretching vibrations of polysulfide (S-S) bonds.

The FTIR spectrum of the produced Ag NPs with a 0.2 mol concentration is illustrated in

Figure 8c. The observed presence of a distinct peak at 1390 cm^{-1} can be ascribed to the (O-H) bending characteristic of an alcohol compound. The presence of two distinct peaks observed at wavenumbers 1184 cm^{-1}, and 1132 cm^{-1} are due to stretching of the (C-N) bond in the amine functional group. The presence of two distinct peaks at 825 cm^{-1}, and 835 cm^{-1} are due to (C=C) bending alkene compound.

Figure 8d displays the FTIR spectrum of Ag NPs synthesized at 0.25 mol concentration. The observed absorption peak at a wavenumber of 1789 cm^{-1} can be attributed to the presence of acid halide, specifically due to the stretching of the carbon-oxygen double bond (C=O). The distinct absorption peak at 1390 cm^{-1} indicates the occurrence of (O-H) bending in an alcohol compound. Additionally, the absorption peak observed at a wavenumber of 2777 cm^{-1} contributes to stretching of the (O-H) bond in an alcohol molecule. The observed peak at 835 cm^{-1} ascribes to the bending of the (C=C) bond in an alkene.

Figure 8e displays the (FTIR) spectra of -(Ag NPs) that were generated using a biosynthetic process with a concentration of 0.3 mol. Similar to the observations made in Figure 8d, the absorption peaks at 1789 cm^{-1}, and 1390 cm^{-1} are evident in the current context, signifying the involvement of the (C=O)

stretching in acid halide and the (O-H) bending in alcohol, respectively. The final absorption peak observed at wavenumber 825 cm^{-1} corresponds to the bending of the (C=C) bond in an alkene molecule.

Finally,

Figure 8e shows the FTIR spectra of biosynthesized Ag NPs at concentration value 0.3 mol. Just like in

Figure 8d, the absorption peaks at 1789 cm^{-1}, and 1390 cm^{-1} are here present and contribute to (C=O) stretching acid halide, and (O-H) bending alcohol, respectively. The last absorption peak obtained at 825 cm^{-1} is (C=C) bending alkene.

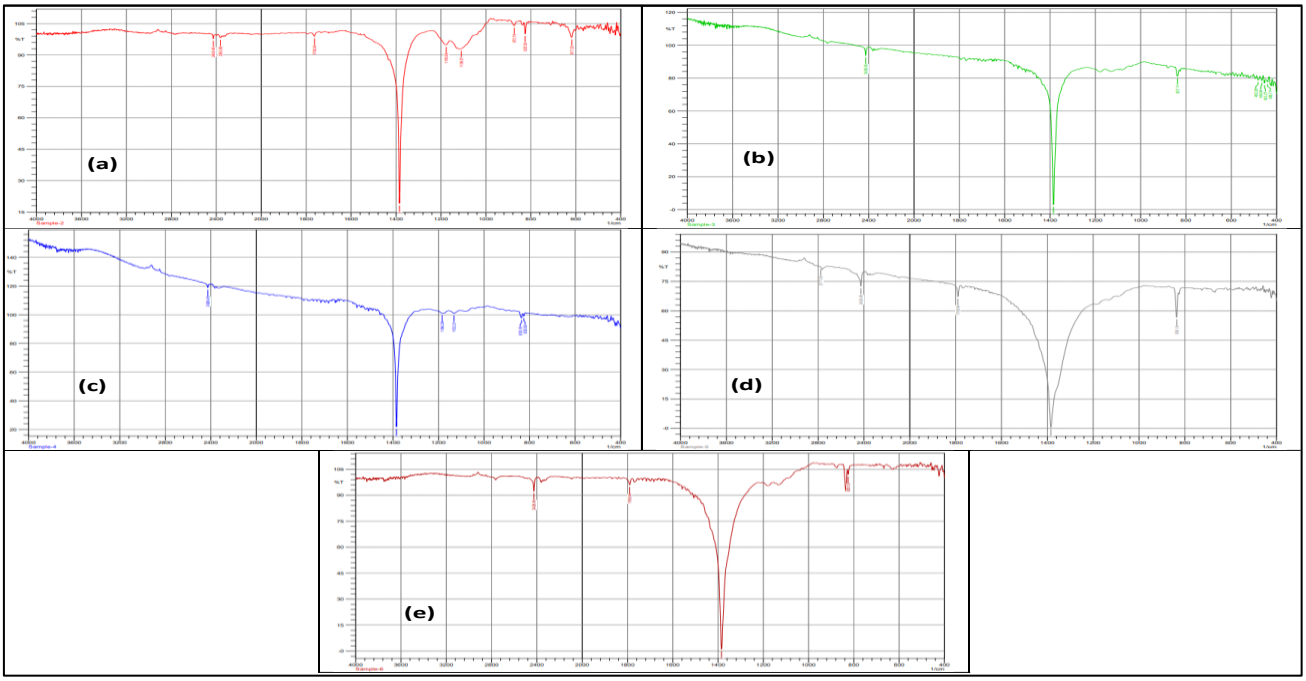

Figure 8: FTIR spectra of Ag nanoparticles generated by green technique and cress (Lepidium Sativum) leaf extract at various concentrations: (a) 0.1 mol, (b) 0.15 mol, (c) 0.2 mol, (d) 0.25 mol, (e) 0.3 mol.

CONCLUSION

High-quality Ag nanoparticles were successfully manufactured utilizing a green method based on leaf extract of the cress plant "Lepidium Sativum." Moreover, the findings revealed that variations in concentration have a noteworthy impact on the crystal structure, and optical properties of (Ag NPs). From the FESEM images, it was seen that the average size of Ag NPs exhibited a decreasing trend as the concentration increased, however a subsequent increase in size was observed at a concentration of 0.3 mol. Additionally, the findings of the FTIR analysis at various concentrations demonstrate the Ag NPs have been produced–from the plant extract. However, all Ag NPs produced by different concentrations exhibit high absorbance in the visible range of UV-Vis' spectra from 430 nm to 460 nm. The energy band gap changed slightly with an increase in concentration and it is obtained that the optical energy band gap for Ag NPs is 2.15 eV. Our outcomes suggest the use of cress plant extract for a rapid, easy, and ecologically friendly manufacture of Ag NPs. The potential applications of these nanoparticles span across multiple domains, including medicine, with a specific focus on anti-cancer treatments and medical applications. Additionally, they hold promise in areas such as disinfectants, food packaging, and wound care products.

REFERENCES:

Naidu, K.S.B., Govender, P. and Adam, J.K., 2015. Nano silver particles in biomedical and clinical applications. *J Pure Appl Microbiol*, *9*, pp.103-112.

Gokarneshan, N. and Velumani, K., 2017. Application of nano silver particles on textile materials for improvement of antibacterial finishes. *Glob. J. Pharmaceu. Sci*, *2*, pp.1-4.

Carbone, M., Donia, D.T., Sabbatella, G. and Antiochia, R., 2016. Silver nanoparticles in polymeric matrices for food packaging.

Naidu Krishna, S., Govender, P. and Adam, J.K., 2015. Nano silver particles in biomedical and clinical applications. *Journal of pure and applied microbiology (Print)*.

Dong, X.Y., Gao, Z.W., Yang, K.F., Zhang, W.Q. and Xu, L.W., 2015. Nanosilver as a new generation of silver catalysts in organic transformations for efficient synthesis of fine chemicals. *Catalysis Science & Technology*, *5*(5), pp.2554-2574.

Thamilselvi, V. and Radha, K.V., 2017. A review on the diverse application of silver nanoparticle. *IOSR J. Pharm*, *7*(01), pp.21-27.

Balamurugan, M., Saravanan, S. and Soga, T., 2017. Coating of green-synthesized silver nanoparticles on cotton fabric. *Journal of Coatings Technology and Research*, *14*(3), pp.735-745.

Oldenburg, S.J., 2014. Silver nanoparticles: properties and applications. *Sigma-Aldrich Co., nd*.

Yue, Q., Wang, L., Fan, H., Zhao, Y., Wei, C., Pei, C., Song, Q., Huang, X. and Li, H., 2020. Wrapping plasmonic silver nanoparticles inside one-dimensional nanoscrolls of transition-metal dichalcogenides for enhanced photoresponse. *Inorganic Chemistry*, *60*(7), pp.4226-4235.

Qasim, M., Udomluck, N., Chang, J., Park, H. and Kim, K., 2018. Antimicrobial activity of silver nanoparticles encapsulated in poly-N-isopropylacrylamide-based polymeric nanoparticles. *International journal of nanomedicine*, *13*, p.235.

Yang, X., Yu, Y. and Gao, Z., 2014. A highly sensitive plasmonic DNA assay based on triangular silver nanoprism etching. *Acs Nano*, *8*(5), pp.4902-4907.

Pulit-Prociak, J. and Banach, M., 2016. Silver nanoparticles–a material of the future…?. *Open Chemistry*, *14*(1), pp.76-91.

Zhang, H., 2013. *Application of silver nanoparticles in drinking water purification*. University of Rhode Island.

Park, K., Seo, D. and Lee, J., 2008. Conductivity of silver paste prepared from nanoparticles. *Colloids and Surfaces A: Physicochemical and Engineering Aspects*, *313*, pp.351-354.

Rafique, M., Sadaf, I., Rafique, M.S. and Tahir, M.B., 2017. A review on green synthesis of silver nanoparticles and their applications. *Artificial cells, nanomedicine, and biotechnology*, *45*(7), pp.1272-1291.

Saif, S., Tahir, A., Asim, T., Chen, Y., Khan, M. and Adil, S.F., 2019. Green synthesis of ZnO hierarchical microstructures by Cordia myxa and their antibacterial activity. *Saudi Journal of Biological Sciences*, *26*(7), pp.1364-1371.

Raveendran, P., Fu, J. and Wallen, S.L., 2003. Completely "green" synthesis and stabilization of metal nanoparticles. *Journal of the American Chemical Society*, *125*(46), pp.13940-13941.

Iravani, S., 2011. Green synthesis of metal nanoparticles using plants. *Green Chemistry*, *13*(10), pp.2638-2650.

Aguş, O., Abalı, Y., Arslan, O. and Keskin, N.O.S., 2019. Facile and controlled production of silver borate nanoparticles. *SN Applied Sciences*, *1*(7), pp.1-8.

Kim, J., Rheem, Y., Yoo, B., Chong, Y., Bozhilov, K.N., Kim, D., Sadowsky, M.J., Hur, H.G. and Myung, N.V., 2010. Peptide-mediated shape-and size-tunable synthesis of gold nanostructures. *Acta biomaterialia*, *6*(7), pp.2681-2689.

Delgado-Mellado, N., Ayuso, M., Villar-Chavero, M., García, J. and Rodríguez, F., 2019. Ecotoxicity evaluation towards Vibrio fischeri of imidazolium-and pyridinium-based ionic liquids for their use in separation processes. *SN Applied Sciences*, *1*(8), pp.1-9.

Dwivedi, A.D. and Gopal, K., 2010. Biosynthesis of silver and gold nanoparticles using Chenopodium album leaf extract. *Colloids and Surfaces A: Physicochemical and Engineering Aspects*, *369*(1-3), pp.27-33.

Gardea-Torresdey, J.L., Gomez, E., Peralta-Videa, J.R., Parsons, J.G., Troiani, H. and Jose-Yacaman, M., 2003. Alfalfa sprouts: a natural source for the synthesis of silver nanoparticles. *Langmuir*, *19*(4), pp.1357-1361.

Shankar, S.S., Ahmad, A. and Sastry, M., 2003. Geranium leaf assisted biosynthesis of silver nanoparticles. *Biotechnology progress*, *19*(6), pp.1627-1631.

Arokiyaraj, S., Arasu, M.V., Vincent, S., Prakash, N.U., Choi, S.H., Oh, Y.K., Choi, K.C. and Kim, K.H., 2014. Rapid green synthesis of silver nanoparticles from Chrysanthemum indicum L and its antibacterial and cytotoxic effects: an in vitro study. *International Journal of Nanomedicine*, *9*, p.379.

Murugan, K., Senthilkumar, B., Senbagam, D. and Al-Sohaibani, S., 2014. Biosynthesis of silver nanoparticles using Acacia leucophloea extract and their antibacterial activity. *International Journal of Nanomedicine*, *9*, p.2431.

Raman, J., Reddy, G.R., Lakshmanan, H., Selvaraj, V., Gajendran, B., Nanjian, R., Chinnasamy, A. and Sabaratnam, V., 2015. Mycosynthesis and characterization of silver nanoparticles from Pleurotus djamor var. roseus and their in vitro cytotoxicity effect on PC3 cells. *Process Biochemistry*, *50*(1), pp.140-147.

Sharma, V., 2019. A Review on Characterization of Solid Dispersion. *Int. J. Eng. Appl. Sci. Technol*, *4*, pp.127-128.

Vidya, C., Hiremath, S., Chandraprabha, M.N., Antonyraj, M.L., Gopal, I.V., Jain, A. and Bansal, K., 2013. Green synthesis of ZnO nanoparticles by Calotropis gigantea. *Int J Curr Eng Technol*, *1*(1), pp.118-120.

Shim, Y.J., Soshnikova, V., Anandapadmanaban, G., Mathiyalagan, R., Perez, Z.E.J., Markus, J., Kim, Y.J., Castro-Aceituno, V. and Yang, D.C., 2019. Zinc oxide nanoparticles synthesized by Suaeda japonica Makino and their photocatalytic degradation of methylene blue. *Optik*, *182*, pp.1015-1020.

Amargeetha, A. and Velavan, S., 2018. X-ray diffraction (XRD) and energy dispersive spectroscopy (EDS) analysis of silver nanoparticles synthesized from Erythrina indica flowers. *Nanosci. Technol. Open Access*, *5*, pp.1-5.

Khalil, M.M., Ismail, E.H., El-Baghdady, K.Z. and Mohamed, D., 2014. Green synthesis of silver nanoparticles using olive leaf extract and its antibacterial activity. Arabian Journal of Chemistry, 7(6), pp.1131-1139.

Melkamu, W.W. and Bitew, L.T., 2021. Green synthesis of silver nanoparticles using Hagenia abyssinica (Bruce) JF Gmel plant leaf extract and their antibacterial and anti-oxidant activities. Heliyon, 7(11), p.e08459.

Shapiro, Adam. (2017). Re: Why small nanoparticles have a better antibacterial activity?why small nanoparticles will give more ion release than big nanoparticles?.

Raza, M.A., Kanwal, Z., Rauf, A., Sabri, A.N., Riaz, S. and Naseem, S., 2016. Size-and shape-dependent antibacterial studies of silver nanoparticles synthesized by wet chemical routes. Nanomaterials, 6(4), p.74.

Ahani, M. and Khatibzadeh, M., 2017. Optimisation of significant parameters through response surface methodology in the synthesis of silver nanoparticles by chemical reduction method. Micro & Nano Letters, 12(9), pp.705-710.

Bloukh, S.H., Edis, Z., Sara, H.A. and Alhamaidah, M.A., 2021. Antimicrobial properties of Lepidium sativum L. Facilitated Silver Nanoparticles. Pharmaceutics, 13(9).

Iftikhar, M., Zahoor, M., Naz, S., Nazir, N., Batiha, G.E.S., Ullah, R., Bari, A., Hanif, M. and Mahmood, H.M., 2020. Green synthesis of silver nanoparticles using Grewia optiva leaf aqueous extract and isolated compounds as reducing agent and their biological activities. Journal of Nanomaterials, 2020, pp.1-10.

Khan, N.T. and Jameel, J., 2016. Optimization of reaction parameters for silver nanoparticles synthesis from Fusarium oxysporum and determination of silver nanoparticles concentration. J Mater Sci Eng, 5(6), pp.6-9.

Mohammadzadeh Kakhki, R., Hedayat, S. and Mohammadzadeh, K., 2019. Novel, green and low cost synthesis of Ag nanoparticles with superior adsorption and solar based photocatalytic activity. Journal of Materials Science: Materials in Electronics, 30(9), pp.8788-8795.

Iftikhar, M., Zahoor, M., Naz, S., Nazir, N., Batiha, G.E.S., Ullah, R., Bari, A., Hanif, M. and Mahmood, H.M., 2020. Green synthesis of silver nanoparticles using Grewia optiva leaf aqueous extract and isolated compounds as reducing agent and their biological activities. Journal of Nanomaterials, 2020, pp.1-10.

Samson, O., Adeeko, T.O. and Makama, E.K., 2017. Synthesis and optical characterization of silver nanoparticles (Ag-NPs) thin films (TFs) prepared by silar technique. Int. J. Curr. Res. Acad. Rev, 5, pp.15-24.

Pantidos, N. and Horsfall, L.E., 2014. Biological synthesis of metallic nanoparticles by bacteria, fungi and plants. Journal of Nanomedicine & Nanotechnology, 5(5), p.1.

Kumar, Dheeraj. (2019). Re: Relation between SPR and Band Gap of Nanoparticles?. Retrieved from: https://www.researchgate.net/post/Relation-between-SPR-and-Band-Gap-of-Nanoparticles/5d5f93d5f8ea52c0902d3d11/citation/download.

Jiang, J., Oberdörster, G., Elder, A., Gelein, R., Mercer, P. and Biswas, P., 2008. Does nanoparticle activity depend upon size and crystal phase?. Nanotoxicology, 2(1), pp.3